International Journal of Thermal Sciences 48 (2009) 1184–1195

Contents lists available at ScienceDirect

International Journal of Thermal Sciences

www.elsevier.com/locate/ijts

Optimal design of a plate heat exchanger with undulated surfaces

A.G. Kanaris, A.A. Mouza, S.V. Paras *

Laboratory of Chemical Process and Plant Design, Department of Chemical Engineering, Aristotle University of Thessaloniki, Univ. Box 455, GR 54124, Thessaloniki, Greece

ARTICLE INFO

Article history:
Received 17 January 2008
Received in revised form 12 September 2008
Accepted 5 November 2008
Available online 28 November 2008

Keywords:
Plate heat exchanger
Sustainable design
CFD
Optimization
Response surface methodology

ABSTRACT

The purpose of this study is to suggest a general method for the optimal design of a plate heat exchanger (*PHE*) with undulated surfaces that complies with the principles of sustainability. A previously validated CFD code is employed to predict the heat transfer rate and pressure drop in this type of equipment. The computational model is a three-dimensional narrow channel with angled triangular undulations in a herringbone pattern, whose blockage ratio, channel aspect ratio, corrugation aspect ratio, angle of attack and Reynolds number are used as design variables. To limit the number of simulations needed, the Box–Behnken technique is employed. An objective function that linearly combines heat transfer augmentation with friction losses, using a weighting factor that accounts for the cost of energy, is employed for the optimization procedure using response surface methodology (*RSM*). New correlations are provided for predicting Nusselt number and friction factor in such PHEs. The results are in very good agreement with published data. Finally, optimal design specifications are suggested for a range of *Re* for two values of the weighting factor.

1. Introduction

The need for designing process equipment that complies with the principles of economic and ecological sustainability (sustainable design) acted as a driving force towards the evolution in the design of plate heat exchangers (*PHE*). The advantages of a PHE over conventional heat transfer equipment also increased their acceptance in two-phase flow applications. They are commonly used in process and power industries for a wide range of temperatures due to their compactness, close temperature approach and ease on inspection and cleaning [1,2]. The plates of these heat exchangers comprise some form of near-sinusoidal corrugations in a herringbone (or chevron) pattern, a design commonly used for PHEs as it is considered the most successful type [3]. It is known [4] that there are two mechanisms for the augmentation of heat transfer, which are also accompanied by pressure loss increase; inducing flow separation and reattachment, and increasing the wall skin friction. When two of these plates are arranged and placed abutting, a channel with complicated passages is formed. Due to the breakup and reattachment of boundary layers, secondary flows and small hydraulic diameter of the flow passages, high heat transfer coefficients are achieved. This allows a small requirement in surface area, up to one third that of a shell-and-tube heat exchanger for a given duty [4], thus reducing the cost, overall volume and space requirement for the exchanger. Nevertheless, the series of periodic changes in flow direction induces a significant resistance to the flow and increases the friction losses. It is therefore apparent that, in order to come up with an optimal design, a 'compromise' between heat transfer and pressure drop must be set. As the plate patterns greatly influence both hydraulic and thermal performance, the final design is certainly dependent on the initial choice of the plate pattern.

The majority of the performance data on this type of equipment are considered proprietary, in a highly competitive PHE market. Thus, the lack of data in open literature has held back the development of a more generic design model for the corrugated plates of a PHE, even though there are studies referring to the effect of several geometrical parameters on the heat transfer coefficient and the friction factor. For instance, Focke et al. [5] and Heavner et al. [6] provide empirical equations based on experimental data regarding the effect of the corrugation inclination angle on the performance of an industrial PHE. Martin [3], in a theoretical approach using the generalized Lévêque equation, provide correlations based on chevron angle for predicting friction factor and Nusselt number in typical PHEs, with limited accuracy (±40%) [4]. Numerical work has also been performed; either on representative elements or in complete conduits. For example, Mehrabian and Poulter [7] study the flow inside a furrow of a PHE with sinusoidal corrugations, while Hossain and Sadrul Islam [8] study similar control volumes for three different corrugation shapes. Moreover, Asako et al. [9] study the case of rounding the corrugations in wavy passages with constant plate spacing using a numerical approach for low Reynolds numbers.

There is an increasing interest on the study of various geometrical parameters of the modulated pattern of the plates with the

* Corresponding author.
E-mail address: paras@cheng.auth.gr (S.V. Paras).

1290-0729/$ – see front matter
doi:10.1016/j.ijthermalsci.2008.11.001

Nomenclature

A	PHE channel area	m^2
A_f	mean cross flow section	m^2
BR	blockage ratio, d/H	
$ChanAR$	channel aspect ratio, H/W	
$CorAR$	corrugation aspect ratio, d/z	
c_p	specific heat capacity	$J\,kg^{-1}\,K^{-1}$
d	height of corrugations	m
D_h	hydraulic diameter	m
F	objective function	
f	friction factor	
f_c	friction factor correction accounting for corrugation shape	
H	half of the channel height	m
h	heat transfer coefficient	$J\,m^{-2}\,K^{-1}\,s^{-1}$
k	thermal conductivity	$J\,m^{-1}\,K^{-1}\,s^{-1}$
L	length of the plate	m
N	number of flow channels per stream	
Nu	overall Nusselt number, based on hydraulic diameter	
P	wetted perimeter	m
Pr	Prandtl number	
Re	Reynolds number based on hydraulic diameter	
T	temperature	K
u	mean entrance velocity	$m\,s^{-1}$
W	half of the channel width	m
y^+	y-plus	
z	width of corrugations	m
$\Delta T_{\ln}$	logarithmic temperature difference	K
ΔP	pressure drop	Pa

Greek

β	weighting factor of the objective function
β_c	weighting factor correction accounting for corrugation shape
η	function
θ	angle of attack (deg)
μ	dynamic viscosity (Pa s)
ρ	density ($kg\,m^{-3}$)
Φ	area enlargement factor

Subscripts

c	cold-fluid stream
f	friction-related term
h	hot-fluid stream
Nu	thermal-related term
0	smooth surface-based term
i	inlet
o	outlet

intention to propose an optimum design of this type of equipment. Kim and Kim [10] seek the optimum design in the case of a rectangular rib-roughened channel placed vertically to the flow direction, while Kim and Lee [11] also use rectangular ribs, but having them placed in a crossed pattern. Zhang et al. [12] check the effect of the fin waviness and spacing for low Reynolds numbers and suggest an optimal design based on these parameters. Wang and Sundén [13] suggest an iterative procedure for determining the optimal design of PHEs with and without pressure drop limitations, taking into account the effect of the corrugation angle. Nevertheless, to the best of author's knowledge, a correlation combining all the design parameters of a PHE is not available in the open literature.

The type of flow inside the passages of a PHE is a significant issue. Focke and Knibbe [14], who performed flow visualization experiments in narrow passages simulating a corrugated PHE, suggest that local flow structure controls the heat transfer process, due to the existence of secondary swirling flow patterns, known as Goertler vortices. The vortices and secondary flows increase turbulence production and help convective processes for heat transfer augmentation by increasing advection of fluid from the center towards the side walls and by producing high shear [4]. Hesselgraves [15] also mention that in plain ducts with polygonal geometries the transition between laminar and turbulent flows is rather sharp. Moreover, Shah and Wanniarachchi [1] acknowledge that there is evidence of turbulent flow even for the low Reynolds number range of 100–1500. The latter statement is also supported by Vlasogiannis et al. [16], who verify that the flow inside an industrial PHE is turbulent for $Re > 650$.

Previous work conducted in this Laboratory [17,18] have proven that CFD is a reliable tool for simulating the operation of PHE. Thus, instead of expensive and time consuming laboratory experiments, CFD simulations can be used for predicting the performance of this type of equipment. The purpose of the present work is to employ numerical simulation as an 'experimental' tool to examine the combined effect of most of the geometrical parameters on the operation of PHE and to check in what extent each of these parameters affects the momentum and heat transfer rate. The ultimate goal is to suggest general correlations for the design of a PHE with corrugations in a herringbone pattern.

2. 'Experimental' procedure

2.1. Selection of design parameters

A series of single three-dimensional channels with triangular ribs in a V-shaped (i.e., herringbone) pattern on both of channel sides is considered for this study. The plates are identical and are placed in a way that a *crossed* pattern is created, as presented in Fig. 1.

The main geometrical parameters (Fig. 2) which, as expected, influence the hydrodynamic behavior of the system are:

- the height (d) and width (z) of the corrugation,
- the height ($2H$) and width ($2W$) of the channel, and
- the angle of attack, theta (θ).

As the corrugation pattern is continuous, (i.e., no gap between the triangular corrugations exists) the width of the corrugation is also the pitch of the repeated modulation pattern.

To perform the simulations, five dimensionless groups are selected as design variables, namely:

- the blockage ratio (BR), defined as d/H, which expresses the percentage of the entrance of the channel that is 'blocked' with corrugations and is also referred to in literature as *rib-to-channel* height ratio [11];
- the channel aspect ratio ($ChanAR$), defined as H/W, which is a measure of how narrow the channel is;
- the corrugation aspect ratio ($CorAR$), defined as d/z, which expresses the obtuseness or acuteness of the triangular corrugation and is also directly related to the area enlargement factor [13];
- the sine of twice the angle of attack ($\sin 2\theta$) which is commonly used by researchers, i.e., Martin [3], in correlations concerning heat transfer and friction losses, and

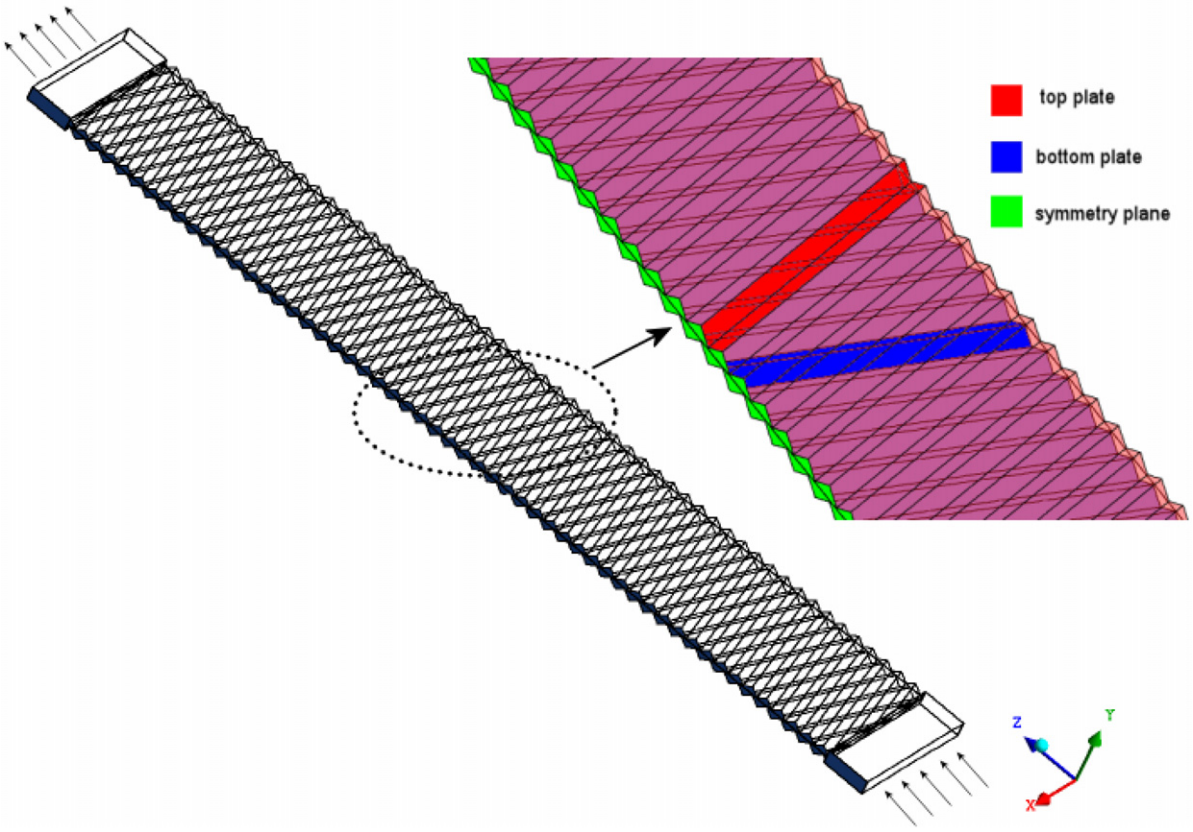

Fig. 1. Computational domain used for the simulations.

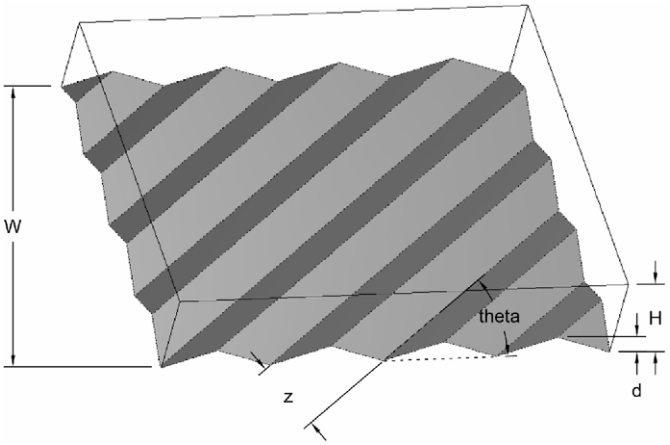

Fig. 2. Geometric parameters of the computational domain.

- the Reynolds number (Re) defined as:

$$Re = \frac{u D_h \rho}{\mu} \tag{1}$$

where u is the mean entrance velocity, ρ and μ the density and dynamic viscosity of the fluid, respectively, and D_h is the hydraulic diameter of the conduit, defined as:

$$D_h = \frac{4A_f}{P} \tag{2}$$

where A_f is the mean cross sectional area and P is the wetted perimeter of the cross-section. In the case of triangular corrugations, the hydraulic diameter can be calculated using the geometrical design parameters, by the following equation:

$$D_h = \frac{2d}{ChanAR + \Phi}\left(\frac{2}{BR} - 1\right) \tag{3}$$

where Φ is the plate area enlargement factor, defined for triangular corrugations (as in the present study) as:

$$\Phi = \left(1 + 4(CorAR)^2\right)^{0.5} \tag{4}$$

Table 1
Constrains of the design variables.

Parameter	Lower limit	Upper limit
BR	0.1	0.9
ChanAR	0.05	0.25
CorAR	0.05	0.40
θ, deg	25	75
Re	500	6000

2.2. Assumptions and simplifications

The design specifications, which are commonly encountered in industrial PHEs, are used to select the bounds of the design variables values in this study, as presented in Table 1. The upper limit of 0.9 on blockage ratio (BR) is imposed by restrictions when creating the grid, as the small gap between the plates stiffens the creation of appropriate grid cells in this area. As the height of the corrugations in a typical PHE is approximately 2 mm, the space between the plates of a channel with $BR = 0.9$ is about 0.2 mm. Therefore, it can be assumed that for $BR = 0.9$, the channel plates are nearly in contact. In the case of corrugation aspect ratio, most PHEs do not typically implement an area enlargement factor, Φ, greater than 1.25 [19], which, according to Eq. (4), equals to a value

of 0.375 for *CorAR*. An upper limit of 0.40 for *CorAR* is set for this study.

It is a known fact that pressure drop in a PHE is very high compared to a shell-and-tube heat exchanger [1]. In the relevant work of Wang and Sundén [13], allowable pressure drop does not exceed 120 kPa. Preliminary simulation results also prove that the pressure drop inside the PHE channel increases above this value for the majority of the geometrical design-variable combinations as *Re* increases, e.g., up to 350 kPa for $Re = 7000$. To keep the pressure drop within acceptable values, as suggested by Shah and Wanniarachchi [1], the *Re* of the flow inside a single PHE channel is set between 500 and 6000.

For the chevron-type PHE, the shape of the corrugation can vary between the sharp shape of the triangular-type and the smooth shape of the sinusoidal-type modulation, depending on the shape of the fabricating tool used to create the corrugations during the manufacturing process. The inclusion of the shape of corrugations as a design variable would further increase the complexity of the optimization problem (in terms of computational demand and optimization method). Kanaris et al. [18] have proven that it is only the pressure drop that is affected by the shape of the corrugations and not the heat transfer rate. Thus, the shape of the corrugations is selected to be triangular for simplicity in constructing the grid for each computational case, while the effect of the corrugation shape on the friction factor will be discussed later in this study.

The working fluid is water and enters the conduit on the *z*-direction (Fig. 1), having an entrance temperature of 40 °C in all simulations. The temperature of the corrugated surfaces is set to a constant value of 20 °C, while all other walls are considered adiabatic. Although the simplification of constant wall temperature seems unrealistic, it allows the designer to focus on the PHE optimization without simulating a second channel for the cold stream, which would lead to an enormous increase in computational demands [18]. A commercial CFD code, namely ANSYS CFX® 10.0, is employed to simulate the flow and to obtain results concerning heat transfer characteristics and pressure drop inside the channel. In the present calculations, the CFD code uses a high resolution advection scheme for the discretization of the momentum equations, while for the pressure-velocity decoupling, a method similar to that by Rhie and Chow is applied [20]. Due to the increased computational demands and to the number of simulations needed, a high performance cluster (HPC) for parallel computing, consisting of six 64-bit AMD processors with a total of 16 GB RAM, is used. The HPC uses Gbit Ethernet connections and runs Gentoo Linux, while the commercial CFD code uses the MPICH protocol for messaging between the nodes. The wall clock time needed for each simulation run varied between 8 and 24 hours, depending on the mesh density of each computational model.

Each computational model with different geometrical details is constructed using the parametric design features of ANSYS Workbench® 10.0. Relevant work in this Lab concerning PHE [17,18] has proven that the SST turbulence model [21] is the most appropriate for simulating the flow inside this type of conduit. More specifically, the SST model activates k–ω model near the wall, where it performs best, while it switches to k–ε for the rest of the flow. As the SST model is basically a two-equation turbulence model, it provides the eddy diffusivity variable in order to express the turbulent fluctuation terms in the Reynolds-averaged transport equations [20]. The quality of the mesh is examined and modified to speed up convergence and increase robustness, while maintaining accuracy in the simulations.

The various grids used for the simulations are unstructured meshes consisting of tetrahedral and prism elements. The tetrahedral elements are created by the ANSYS ICEM CFD® Mesher using the Delaunay method [20]. In order to facilitate the boundary layer calculations, a layer of prism elements (also known as 'inflated' elements) is imposed in the vicinity of the walls. This procedure is necessary for confined geometries [20] in order to create elements with y^+ smaller than 1.0 near the corrugated wall, as imposed by the SST model. As the flow is symmetrical with respect to the *yz*-plane and to keep the memory requirements low, the final computational model represents *half* the actual channel (Fig. 1). Steady-state condition is set for all simulations. Fig. 3 presents typical results of temperature and pressure drop distribution in the channel. The results are finally expressed in terms of local and overall Nusselt number and friction factor.

3. Quest for the optimal design

3.1. Optimization method

The optimal solution for a V-shaped PHE is obtained using a polynomial-based Response Surface Method (RSM), a global optimization method that includes a collection of techniques, i.e., design of experiments (DOE), regression analysis and analysis of variance (ANOVA) techniques [22]. The DOE techniques allow the designer to extract as much information as possible from a limited number of test cases. For example, for the case of five design factors, a three-level full factorial design would require 243 design (or training) points compared to the 41 design points required by the Box–Behnken, a common DOE technique. This method is ideal for CFD cases, where a single simulation can take hours or even days to run.

Using a DOE technique, a series of experiments or numerical simulations are performed for a prescribed set of design points, in order to construct a response surface of the measured quantity over the design space, i.e., a function $\eta(x_1, x_2, \ldots, x_n)$, where $x_1, x_2, \ldots, x_n$ are the design variables with values constrained in specific ranges. When a second-order polynomial is used, the response surface equation is expressed as:

$$\eta = a_0 + \sum_{j=1}^{n} a_j x_j + \sum_{j=1}^{n} a_{jj} x_j^2 + \sum \sum_{i \neq j}^{n} a_{ij} x_i x_j \tag{5}$$

where α_{ii} are the unknown coefficients of the polynomial equation determined using the calculated values of the measured quantity for the prescribed set of design points. This equation, η, is also referred to as a *quadratic model*. A set of training points is selected using a Box–Behnken design and is presented in Table 2. The Box–Behnken design method is valid for use in RSM as it is proven [23] that it is sufficient to fit a quadratic model. Each independent variable is placed at one of three equally spaced values – low, center and high value (as in a three-level full factorial design) – and the ratio of the number of training points to the number of coefficients of the quadratic model is kept between 1.5 and 2.6. A certain number of factors are put through all combinations for the factorial design, while the other factors are kept to their center values. This type of DOE technique ensures that factors will not be set to their high levels simultaneously and thus avoids extreme factor combinations [24].

The RSM has been successfully used in several attempts to optimize a compact heat exchanger [10,11,25,26]. A common method for testing the significance of a response surface model is the adjusted coefficient of determination, R^2_{adj}. It is suggested that, when $0.9 \leqslant R^2_{adj} \leqslant 1$, the value of the objective function is accurately predicted by the response surface model [10].

3.2. Definition of the objective function

To optimize the PHE performance, a function that incorporates both the enhancement of heat transfer and the increase of friction losses must be formulated [27]. All the other cost factors, i.e.,

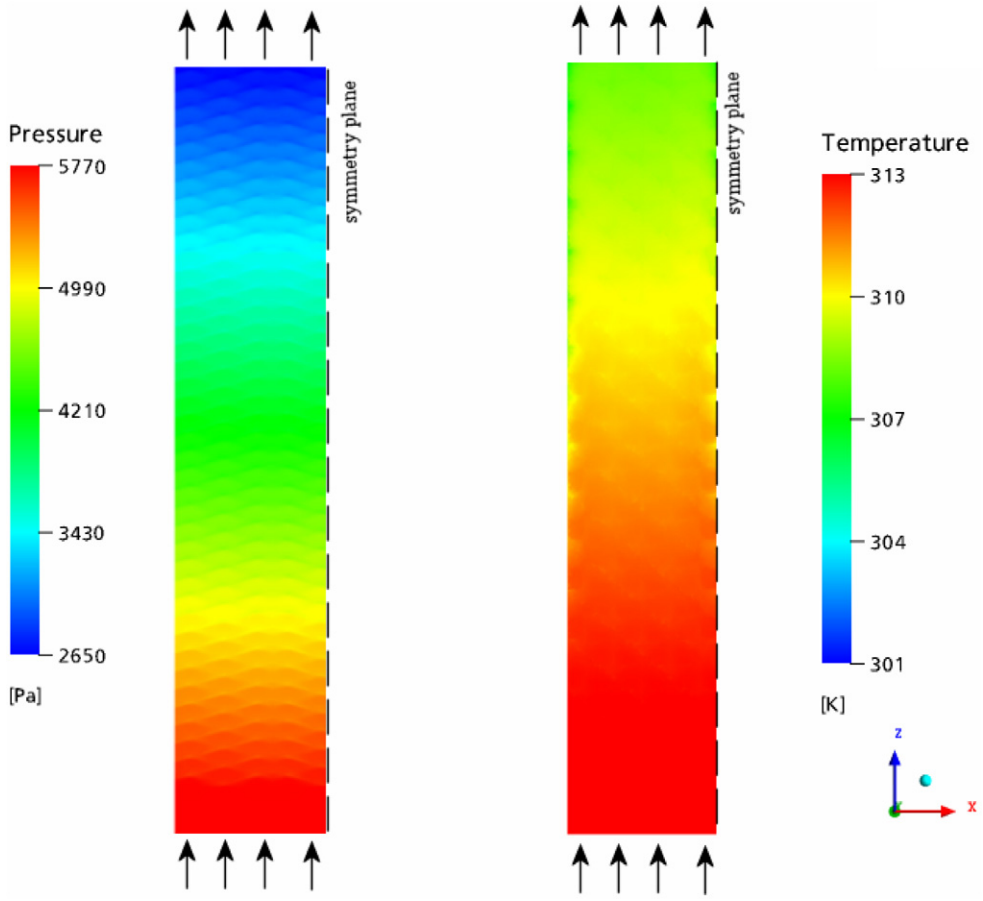

Fig. 3. Typical pressure and temperature distributions across a corrugated plate.

equipment, maintenance and labor cost are not practically affected by the geometry of the PHE. Consequently, a *thermal-related function* (η_{Nu}) that gives the heat transfer augmentation with respect to that for a smooth surface, is defined as:

$$\eta_{Nu} = \left(\frac{Nu}{Nu_0}\right)^{-1} \tag{6}$$

The overall Nusselt number Nu is defined as:

$$Nu = \frac{hD_h}{k} \tag{7}$$

where D_h is the hydraulic diameter of the conduit, k the average thermal conductivity and h the average heat transfer coefficient predicted by the simulation. Nu_0 is the Nusselt number for fully-developed flow in a smooth pipe and is calculated by the Dittus–Boelter correlation [15]:

$$Nu_0 = 0.023Re^{0.8}Pr^{0.3} \tag{8}$$

where Pr is the Prandtl number. Accordingly, a *friction-related function* (η_f), which expresses the increase of friction losses with respect to that for a smooth surface is defined as:

$$\eta_f = \left(\frac{f}{f_0}\right)^{1/3} \tag{9}$$

where the friction factor, f, is given by:

$$f = \frac{\Delta P}{L}\frac{D_h}{\rho u^2/2} \tag{10}$$

where $\Delta P/L$ is predicted by the simulation. The friction factor for smooth circular tube, f_0, is calculated by [15]:

$$f_0 = \frac{64}{Re}, \qquad Re < 2300 \tag{11}$$

$$f_0 = (1.8\log Re - 1.5)^{-2}, \qquad Re \geqslant 2300 \tag{12}$$

Each of the functions is expressed as a *quadratic* model of the five design variables (Table 1), using the RSM. Finally, the aforementioned two functions are linearly combined in an *objective function*, F, which compromises between the heat transfer augmentation and the inevitable increase of friction losses [27]:

$$F = \eta_{Nu} + \beta\eta_f \tag{13}$$

where the parameter β is a weighting factor that accounts for the pumping cost to thermal energy cost and can be estimated using data concerning the cost of a unit of heat produced by a common fuel (e.g., natural gas) and the cost of the same amount of electric energy. The definition of these two functions is suggested [28] and used [10,11] in the literature for this optimization approach. The linear combination of two factors concerning the heat transfer augmentation and the corresponding friction losses is also mentioned in the fundamental work of Bejan et al. [29]. According to literature, β varies between 0 and 0.1 [10]. For the purpose of this study, results are presented for various Re and for two values of the weighting factor, i.e., 0.03 and 0.06, where 0.03 corresponds to the present day conditions in Greece, and the effect of the weighting factor on the values of the optimal design parameters is discussed.

Therefore, to maximize the performance of the type of PHEs in question, the objective function defined above should be *minimized*.

Table 2
Prescribed set of design points using the Box–Behnken technique.

BR	*ChanAR*	*CorAR*	θ, deg	*Re*
0.5	0.15	0.225	50	3250
0.5	0.05	0.225	50	3250
0.5	0.05	0.225	50	3250
0.1	0.05	0.225	50	3250
0.5	0.15	0.400	50	3250
0.5	0.25	0.400	50	3250
0.1	0.15	0.225	50	3250
0.5	0.15	0.225	75	3250
0.5	0.25	0.225	25	500
0.5	0.15	0.225	25	500
0.5	0.25	0.225	50	6000
0.1	0.25	0.225	50	6000
0.5	0.15	0.050	75	3250
0.5	0.25	0.050	50	3250
0.5	0.05	0.400	50	3250
0.5	0.15	0.400	50	3250
0.9	0.15	0.050	50	500
0.5	0.15	0.225	75	500
0.9	0.15	0.400	50	6000
0.5	0.05	0.225	75	6000
0.9	0.15	0.225	75	3250
0.5	0.05	0.225	25	3250
0.1	0.15	0.225	25	3250
0.9	0.15	0.225	25	3250
0.1	0.15	0.400	50	3250
0.9	0.05	0.225	50	3250
0.5	0.15	0.400	75	3250
0.5	0.25	0.225	50	3250
0.5	0.15	0.225	25	500
0.9	0.15	0.225	50	500
0.5	0.15	0.050	50	6000
0.5	0.25	0.225	75	6000
0.1	0.15	0.225	75	500
0.5	0.05	0.050	50	500
0.9	0.15	0.225	50	6000
0.5	0.15	0.050	50	6000
0.1	0.15	0.050	50	3250
0.5	0.15	0.400	25	3250
0.5	0.15	0.050	25	3250
0.9	0.25	0.225	50	3250
0.1	0.15	0.225	50	3250

Table 3
Values of the coefficients of the quadratic models for: (a) η_{Nu}, (b) η_f.

(a)						
η_{Nu}	1	*BR*	*ChanAR*	*CorAR*	$\sin 2\theta$	*Re*
1	−0.00220					
BR	−0.05756	0.31230				
ChanAR	−0.28845	−0.72577	6.10191			
CorAR	−1.41326	−1.40661	−1.06706	4.58153		
$\sin 2\theta$	0.94572	0.10292	−0.59416	−0.27910	−0.57396	
Re	1.56E−05	−1.30E−05	5.51E−05	−7.67E−05	−1.64E−05	4.90E−09
(b)						
η_f	1	*BR*	*ChanAR*	*CorAR*	$\sin 2\theta$	*Re*
1	5.35675					
BR	1.31185	3.34690				
ChanAR	3.15423	−0.40463	−8.15968			
CorAR	−8.86597	2.47967	−10.92780	2.14140		
$\sin 2\theta$	−12.19970	−2.24776	−0.83843	12.66120	7.51322	
Re	7.92E−4	2.00E−4	−5.74E−5	1.22E−3	−1.05E−4	−8.28E−08

4. Results and discussion

The coefficients of the quadratic models for the thermal-related, η_{Nu}, and the friction-related, η_f, functions were calculated using the RSM and are presented in Table 3. For both functions, the adjusted coefficient of determination, R^2_{adj}, is found to be greater than 0.9. The η_{Nu} and η_f functions are used for the calculation of Nusselt number, *Nu*, and friction factor, f.

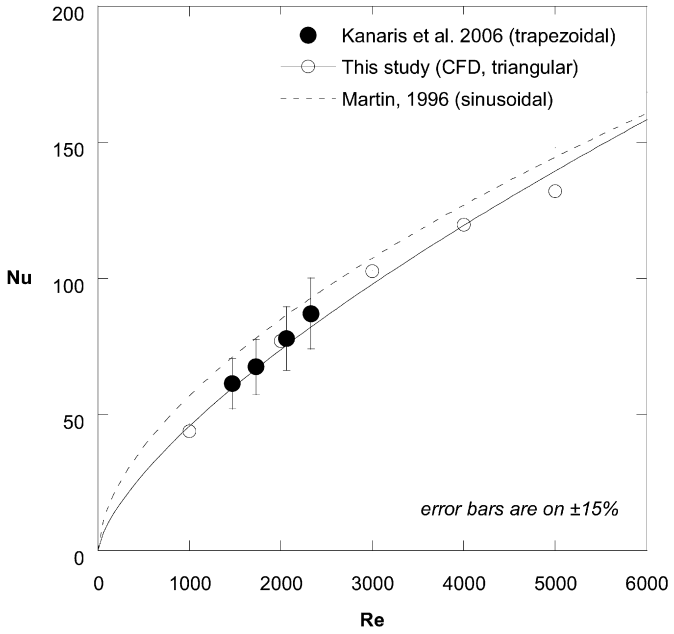

Fig. 4. Nu vs Re for different corrugation shapes.

4.1. Nusselt number estimation

The validity of the proposed correlation for Nusselt number estimation is checked using limited experimental data [18]. It is also compared with the most popular correlation available in the literature, proposed by Martin [3]. In Fig. 4, the proposed plotted correlation for the *Nu* refers to a PHE channel with the same geometrical configuration as the one used in the experimental setup by Kanaris et al. [18] and found to be in excellent agreement. Comparison with the correlation by Martin, used for a given angle of attack ($\theta = 67°$), shows that the two correlations are in good agreement (±20%). It must be noted that Martin's correlation [3] takes into account only the angle of attack. An interesting observation is that the difference on the corrugation shape does not seem to affect the *Nu* values, i.e., the proposed correlation refers to triangular, available experimental data refer to rounded trapezoidal and Martin's correlation refers to sinusoidal corrugations.

4.2. Friction factor estimation

In a similar way, the validity of the proposed correlation for friction factor is checked using available experimental data [18] and is also compared with the correlation available in the literature, proposed by Martin [3]. In Fig. 5, four different groups of data are presented. More specifically:

- data from the proposed correlation, referring to triangular corrugations,
- data from CFD simulations concerning trapezoidal corrugations [18],
- experimental data corresponding to rounded trapezoidal corrugations [18] and finally,
- data calculated by the correlation of Martin [3] which concerns sinusoidal corrugations.

It is obvious that the sharpness of the corrugation influences the friction factor values, i.e., the sharpest the corrugation, the higher the friction factor. However, all data groups are well fitted with a power law function, as suggested by Martin [3], with the value of −0.135 being the exponent of *Re*.

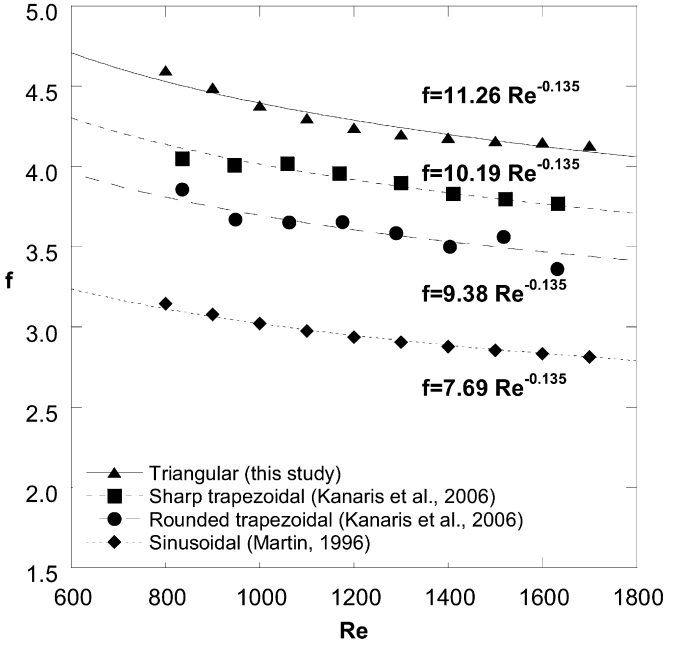

Fig. 5. Friction factor vs. Re for different corrugation shapes.

Table 4
Friction factor correction and weighting factor correction for each shape case.

	K ($f = KRe^{-0.135}$)	Friction correction factor, f_c	Weighting factor correction, $\beta_c = f_c^{1/3}$
Triangular	11.26		
Sinusoidal	7.69	0.68	0.88
Rounded trapezoidal	9.38	0.83	0.94
Sharp trapezoidal	10.19	0.90	0.97

Consequently, a correction factor, f_c, calculated as a ratio of friction factor for one of the aforementioned shapes (i.e., sinusoidal, rounded trapezoidal or sharp trapezoidal) over the friction factor for the case of triangular shaped corrugations, can be used to account for the corrugation shape. The proposed values for the correction factor are presented in Table 4.

4.3. Optimization results

In general the values of the four geometrical design variables and the *Re* number which correspond to the optimal design are calculated by the aforementioned method. Keeping *Re* constant, the objective function is repeatedly optimized with respect to the four geometrical parameters used as design variables for various *Re* values. This allows the designer to use the correlations derived in this study to check the effect of *Re* on the optimal parameter values and to design the best PHE for each case. The aforementioned correlations can also be used for the calculation of the optimal design specification when the value of any of the geometrical parameters is pre-set (e.g., $BR \simeq 1$ or $\theta = 45°$).

As previously mentioned, the optimization of Eq. (13) has been performed for various values of *Re* and for two values of the weighting factor, β, 0.03 and 0.06, in order to find the geometrical configuration that provides the most efficient design. The values of the geometrical parameters that correspond to this optimal design are presented in Fig. 6 and are also tabulated in Table 5.

It is obvious that the pumping cost, incorporated in the weighting factor, plays a significant role. As shown in Fig. 6, when $\beta = 0.03$, it is apparent that the optimal values of the geometrical parameters are practically constant for the range of *Re* studied (i.e., the plates must be placed abutting, $\theta \simeq 40^0$, $CorAR = 0.40$ and

Table 5
Optimal values of design geometrical parameters for $\beta = 0.03$ and 0.06.

	$\beta = 0.03$				$\beta = 0.06$			
Re	*BR*	*ChanAR*	*CorAR*	θ	*BR*	*ChanAR*	*CorAR*	θ
500	0.900	0.226	0.400	41.2	0.771	0.250	0.393	38.6
1000	0.900	0.222	0.400	41.2	0.755	0.242	0.386	39.1
2000	0.900	0.216	0.400	41.7	0.666	0.203	0.340	42.2
3000	0.900	0.212	0.400	41.7	0.641	0.189	0.326	42.7
4000	0.900	0.206	0.400	42.2	0.617	0.171	0.308	43.2
5000	0.900	0.200	0.400	42.7	0.593	0.163	0.298	43.7
6000	0.900	0.196	0.400	42.7	0.585	0.153	0.287	44.2

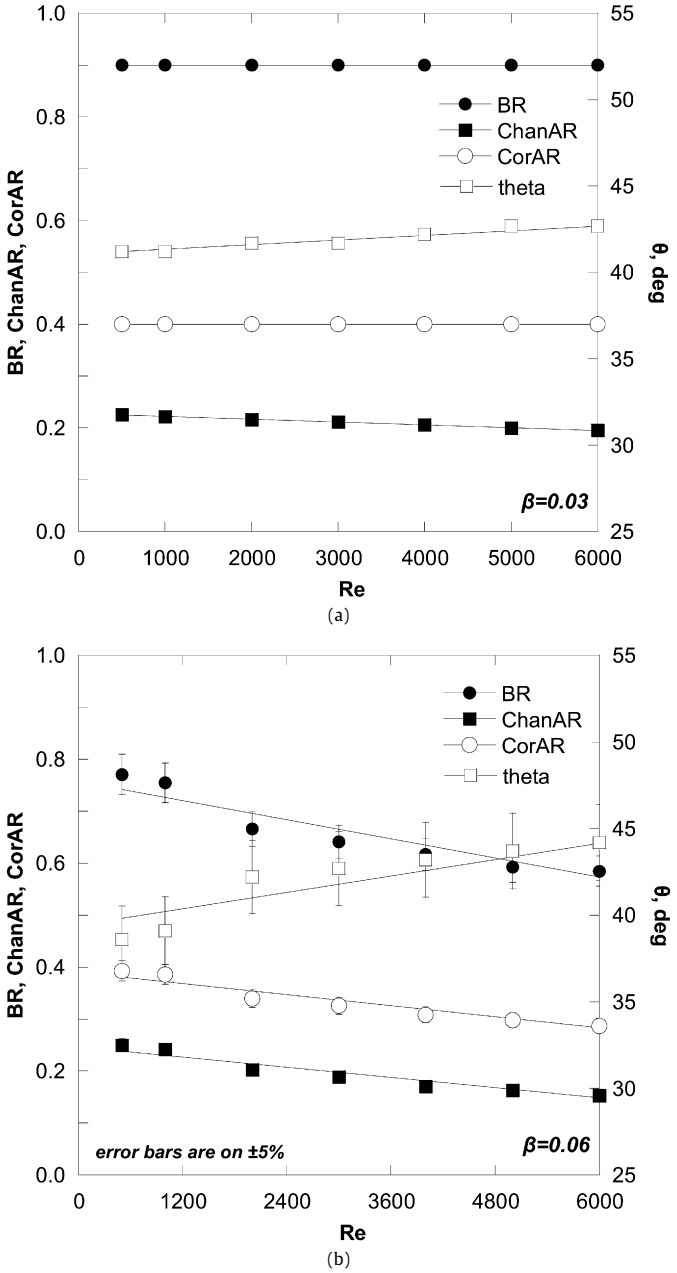

Fig. 6. Optimal values of design geometrical parameters using CFD, for: (a) $\beta = 0.03$ and (b) $\beta = 0.06$.

ChanAR $\simeq 0.20$). However, for $\beta = 0.06$ (i.e., pumping cost is more significant), the values of the design variables for the optimal design of a PHE, not only differ from the previous values, but they are also a function of *Re*. Since, in this case, the friction losses have a greater effect on the objective function values, an optimal

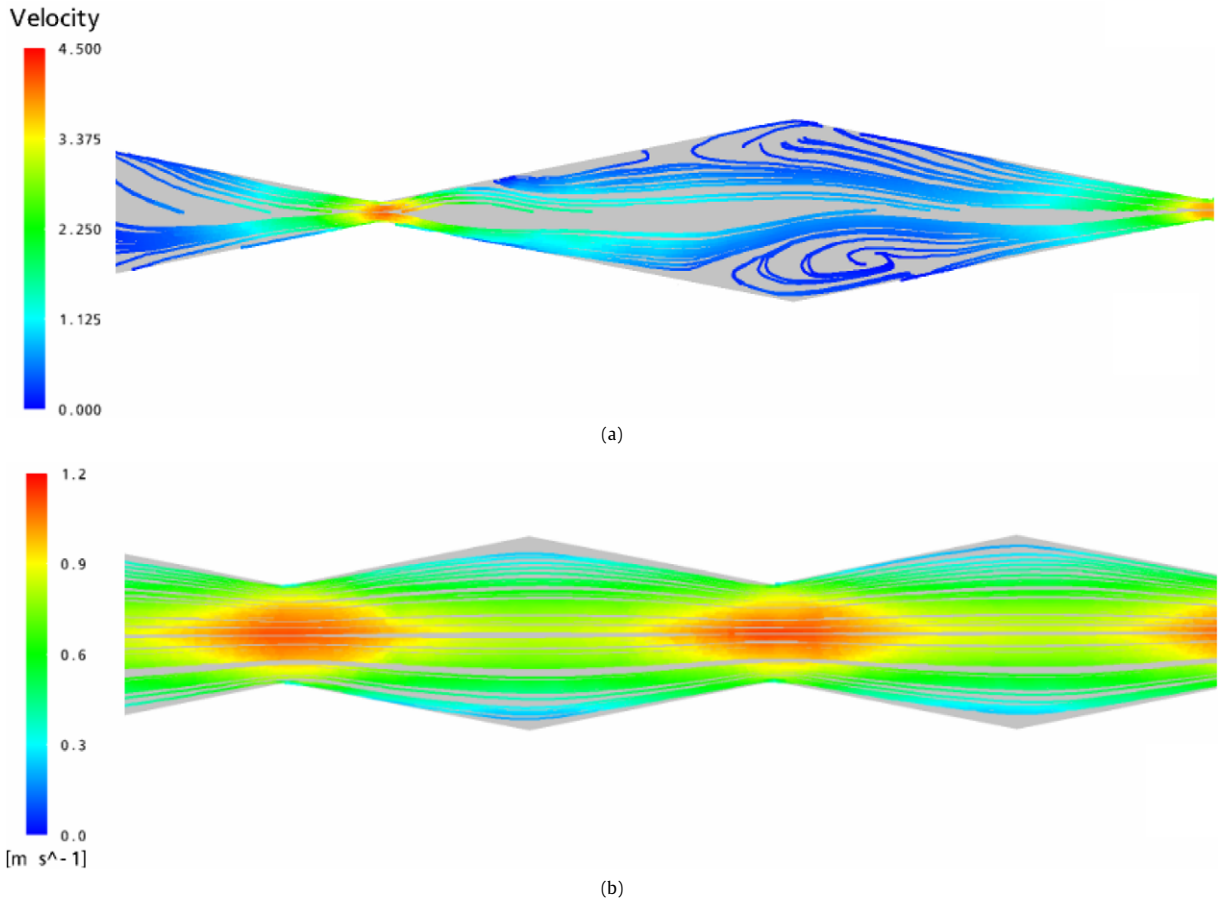

Fig. 7. Boundary layer breakup and reattachment of the flow on a cross section of a channel ($ChanAR = 0.15$, $CorAR = 0.225$, $\theta = 75$, $Re = 3250$) for: (a) $BR = 0.9$ and (b) $BR = 0.5$.

design leads to greater distances between the plates (a behavior also mentioned in the similar work by Kim and Kim [10]) and less sharp corrugations (i.e., smaller values of *BR* and *CorAR*).

The effect of the distance between the plates, which is expressed by *BR*, is presented in Fig. 7 for the case of two closely placed plates (Fig. 7a, $BR = 0.9$) and for the case that the plates are located in some distance apart from each other (Fig. 7b, $BR = 0.5$), all other parameters being the same ($ChanAR = 0.15$, $CorAR = 0.225$ and $\theta = 75°$). It is obvious that, when the plates are placed abutting, the type of flow inside the channel greatly affects the heat transfer augmentation and the friction losses, due to the 'restart' of the boundary layer.

As for the angle of attack, θ, while for low *Re* the optimal design leads to 'soft' plates (i.e., with small angles, $\theta = 30°–40°$), for higher *Re* the optimal values are shifted to geometrical configurations with greater angles ('harder' plates) on the corrugation pattern. This is in agreement with Martin [3], who observes that, for a given pressure drop, 'harder' plates result to higher temperature changes. In Fig. 8a and b, the type of flow inside a channel is presented for two different corrugation angles, i.e., $\theta = 75°$ and $\theta = 25°$, respectively, while all the other geometrical parameters retain the same values (i.e., $BR = 0.9$, $ChanAR = 0.25$ and $CorAR = 0.40$). It is shown that the flow reattachment length is greater for higher values of the angle of attack. It is noted that in Fig. 8a and b, the different angles of attack and the fact that the cross sections lie on a plane parallel to the flow create the illusion of different *CorAR*. It is obvious that on 'harder' plates the 'restarts' of boundary layer are more frequent, contrary to the case of low angles of attack.

In the case of *CorAR*, the increase of the parameter value leads to an increase on the reattachment length. This is apparent in Fig. 8a and c, where the type of flow is presented for two *CorAR* values, 0.40 and 0.15, for $BR = 0.9$, $ChanAR = 0.25$, $\theta = 75°$ and $Re = 500$. For low values of the weighting factor (e.g., $\beta = 0.03$) the effect of this parameter on the overall energy economy is insignificant (Fig. 6a), whereas for $\beta = 0.06$ the optimal *CorAR* value decreases with *Re* (Fig. 6b) and is always smaller than that for $\beta = 0.03$ (Table 5). In the work of Kim and Kim [10], it is stated that *CorAR* reaches its highest value as the weighting factor decreases, in agreement with the results of the present study. In Fig. 9, it is shown that friction losses increase linearly with *CorAR*. The upper limit of the design variable used for the calculations is imposed by PHE construction constrains, as mentioned earlier. Nevertheless, in cases of low pumping cost (i.e., low values of β) the designer could explore the use of sharper corrugations.

Optimal values of *ChanAR*, the variable that expresses how narrow or wide the PHE channel is, decreases with *Re* (for the *Re* range studied). This parameter represents the effect of the side walls on the performance of the PHE. It is reported that two kinds of flow occur in the PHE: the 'crossing flow' and the 'zig-zag flow' [5]. During crossing flow (Fig. 10a), small sub-streams follow the furrows of the corrugated plates, while, during 'zig-zag flow' (Fig. 10b), the fluid 'walks' over the corrugations, by rapidly changing direction. It is known [5] that the wall shear stress attains its peak values on the crests of the corrugations, resulting in increased heat flux, and this study confirms this behavior (Fig. 11). Therefore, when the flow is forced to follow the 'zig-zag flow', friction losses increase. Existence of 'crossing-flow' in this type of equipment is one of the results of the reflection of fluid flowing in the

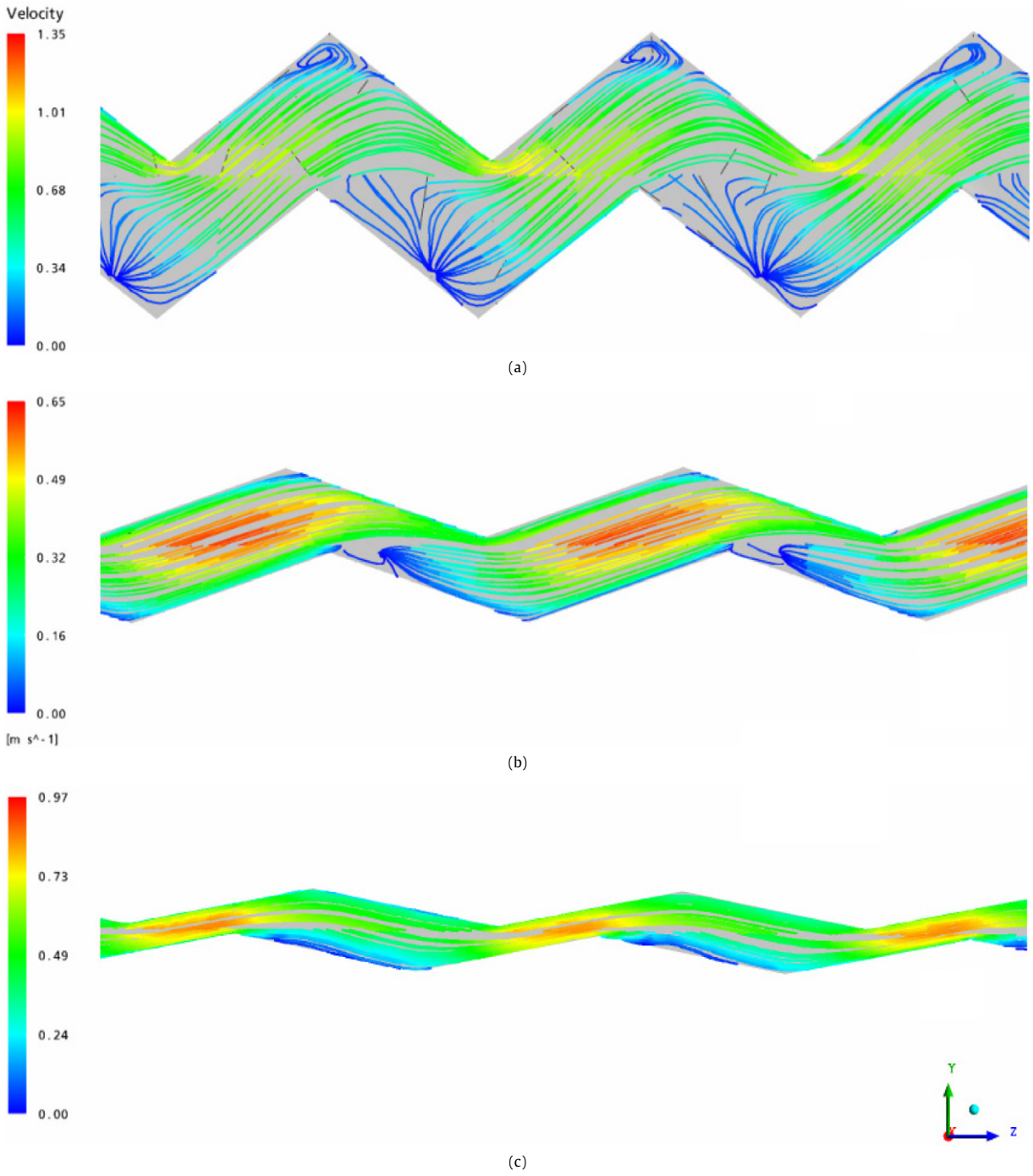

Fig. 8. Boundary layer breakup and reattachment of the flow on a cross section of a channel (*ChanAR* = 0.25, *BR* = 0.9, *Re* = 500) for: (a) *CorAR* = 0.40, $\theta = 75°$, (b) *CorAR* = 0.40, $\theta = 25°$ and (c) *CorAR* = 0.15, $\theta = 75°$.

furrows upon channel side walls. For a channel with low *ChanAR* (i.e., 'wide' channel) reflections on side walls become less frequent, because for long furrows, part of the flow inside them tends to change direction and to follow the 'zig-zag flow' pattern. As the weighting factor increases, the optimal value of *ChanAR* reaches higher values, resulting in narrower channels, where pressure drop decreases.

4.4. Effect of weighting factor

The optimal values of the objective function have been also calculated for various values of the weighting factor β and for two typical *Re* (1000 and 5000) and are presented in Fig. 12. It is shown that the geometrical parameter values that correspond to the optimal design remain practically unaffected when $\beta < 0.04$. If β exceeds 0.04, the friction-related term seems to become the controlling step of the optimization, and leads to geometrical configurations with lower pressure drop.

It must be pointed out that, the corrugation-shape correction factor (f_c) is raised to the 1/3 power when it is included in the objective function and thus its significance on the objective function values is reduced (Eq. (9)). So finally a new weighting factor can be defined, which is the product of β and β_c, where $\beta_c = f_c^{1/3}$ (Table 4) and the objective function for optimization becomes:

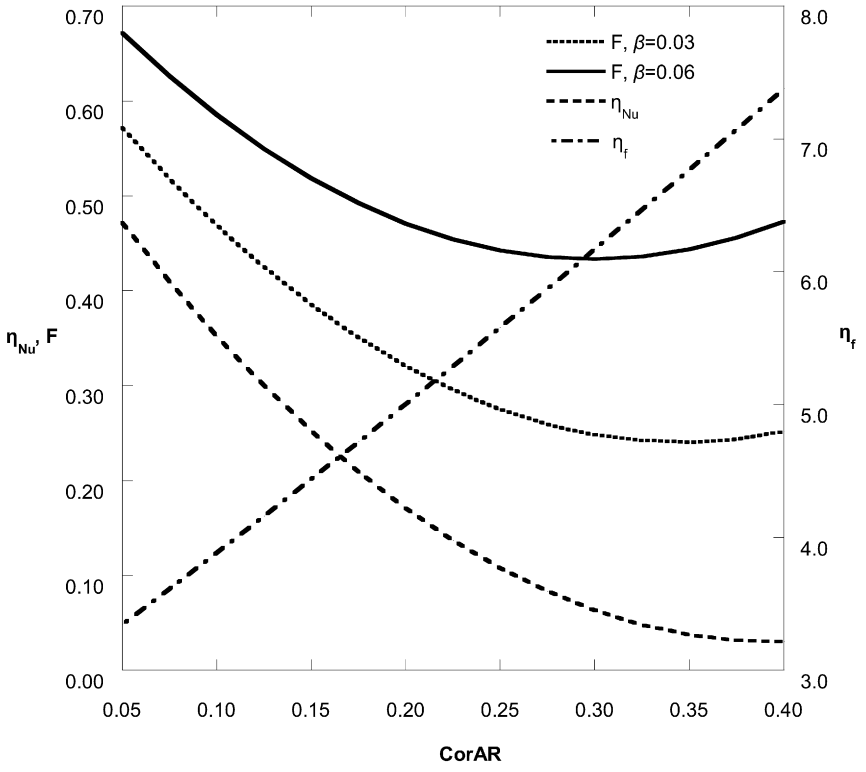

Fig. 9. Effect of *CorAR* on the values of the thermal and friction related functions, for $BR = 0.5$, $ChanAR = 0.15$, $\theta = 50^{\circ}$ and $Re = 6000$.

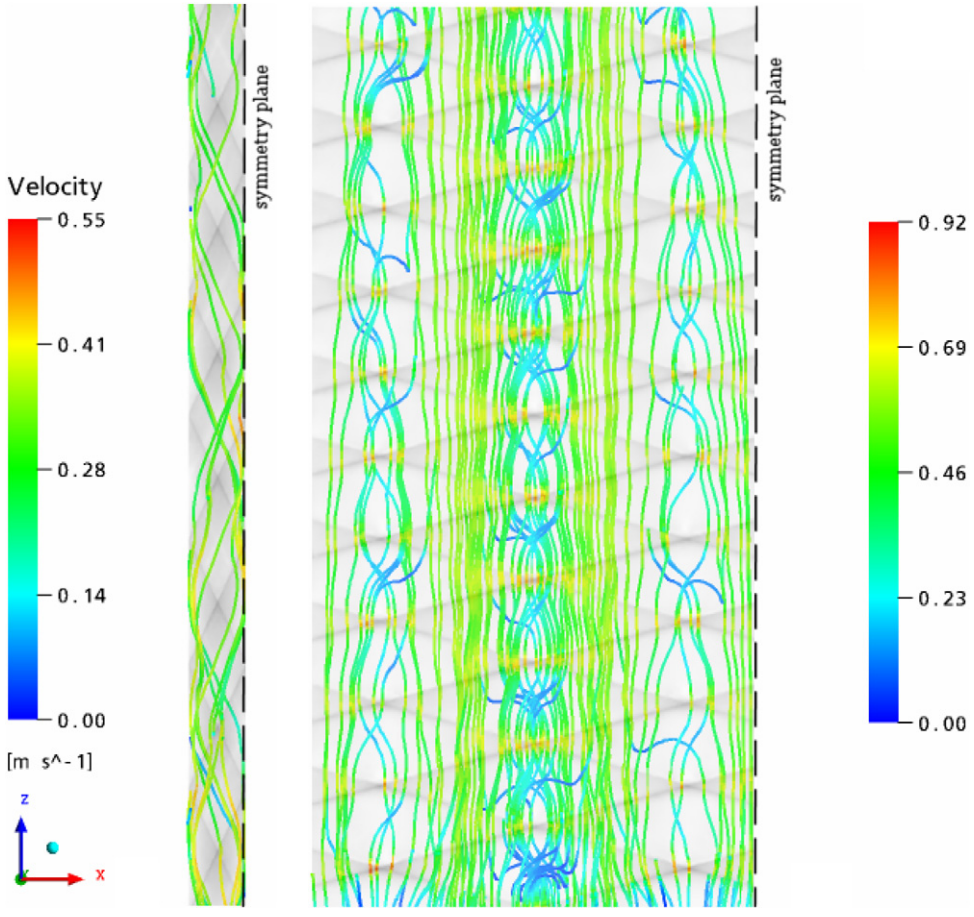

Fig. 10. Flow streamlines presented for different channel aspect ratio: (a) $ChanAR = 0.25$ (narrow channel), (b) $ChanAR = 0.05$ (wide channel).

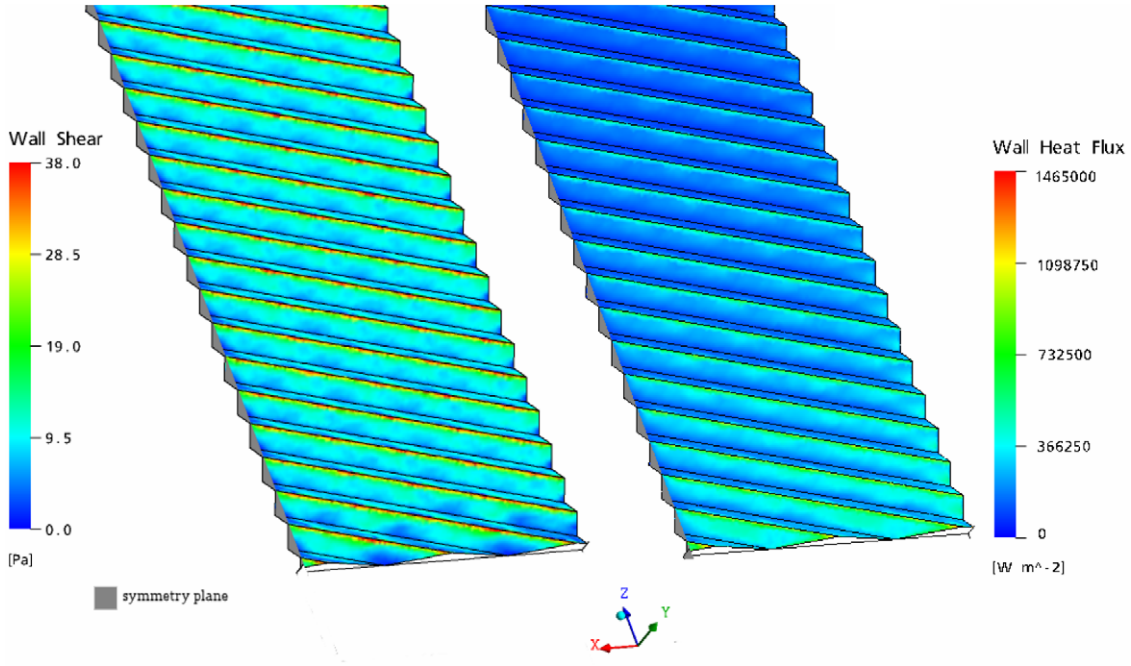

Fig. 11. Shear stress and heat flux distribution on the corrugated plate.

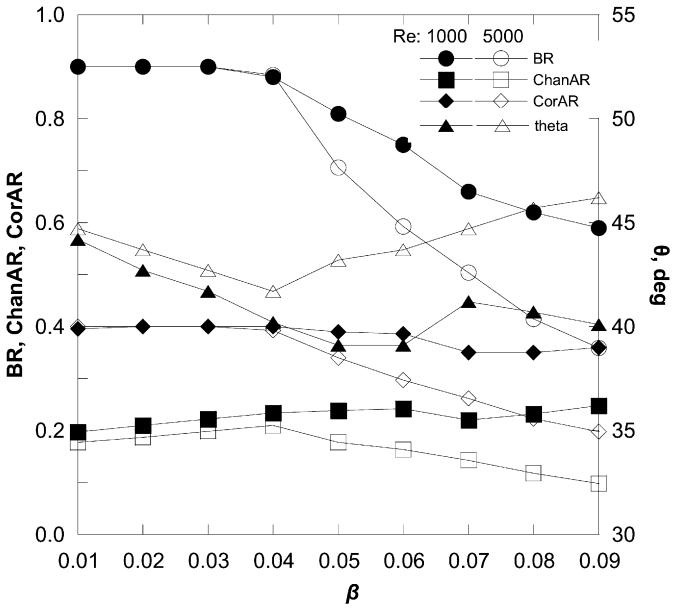

Fig. 12. Optimal values of design geometrical parameters vs the weighting factor for $Re = 1000$ and $Re = 5000$.

$$F = \eta_{Nu} + (\beta \cdot \beta_c)\eta_f \tag{14}$$

It is interesting that even for the smoothest shape (i.e., sinusoidal) the effect of the correction factor would be about 10%. This correction factor is also assumed to be independent of *BR*.

5. Conclusions

A commercial CFD code validated previously by experimental work in our Lab is used for the calculation of heat transfer rate and friction losses in a channel of a PHE with undulated surfaces. This study extends the use of CFD for seeking the optimal design for this type of equipment. Results presented in this study consider the use of water as working fluid. The response surface methodology (RSM) is used as a global optimization method and results are presented in terms of Nusselt number and friction factor. Box–Behnken design was selected for the four geometrical design factors and the Reynolds number to construct the response surface. Results from the CFD simulations show very good agreement with correlations for this type of industrial PHE from the literature as well as with available experimental data. An objective function is appropriately defined as a linear trade-off between heat transfer and pressure drop, combined with a weighting factor accounting for the cost of energy. The correlations proposed for the calculation of heat transfer rate and friction losses can be considered a valuable tool for the optimal design of a PHE. Additionally, the designer can independently choose which of the five available degrees of freedom to use as design variables to optimize a PHE.

More specifically, it is shown that optimal performance is achieved as the channel plates are coming closer to each other and for less obtuse (i.e., sharper) corrugations, while the PHE performance can be improved for lower values of channel aspect ratio (i.e., wider channels) and for higher values of the angle of attack, as *Re* increases. In all cases, the designer can be led to the optimal geometrical configuration of a PHE with the use of values of design parameters that create intense flow inside the furrows, a case where secondary flow due to the corrugations is dominant. This secondary flow increases flow separation and reattachment, which is a known mechanism that improves heat transfer augmentation. As the weighting factor increases, meaning that the friction losses play a very important role, the optimal design of a PHE dictates greater distances between the plates and less sharp corrugations, for high values of *Re*. More work can be done to check the effect of flow configuration in the geometrical parameter values that optimize the performance of a PHE complying with the principles of ecological and economic sustainability.

Acknowledgements

Financial support by the General Secretariat for Research and Technology and the European Union (PENED 2003) is greatly acknowledged. The authors wish to thank Prof. V. Bontozoglou, Prof. S.G. Yiantsios and Prof. N. Sahinidis for their helpful comments and suggestions.

References

[1] R.K. Shah, A.S. Wanniarachchi, Plate heat exchanger design theory, in: J.M. Buchlin (Ed.), Industrial Heat Exchangers, von Karman Institute Lecture Series, 1991.

[2] W.M. Kays, A.L. London, Compact Heat Exchangers, 3rd ed., Krieger Publ. Co., Florida, USA, 1998.

[3] H. Martin, A theoretical approach to predict the performance of chevron-type plate heat exchangers, Chem. Eng. Proc. 35 (1996) 301–310.

[4] R.K. Shah, D.P. Sekulić, Fundamentals of Heat Exchanger Design, John Wiley and Sons, Inc., Hoboken, NJ, 2003.

[5] W.W. Focke, J. Zachariades, I. Olivier, The effect of the corrugation inclination angle on the thermohydraulic performance of plate heat exchangers, Int. J. Heat Mass Transfer 28 (1985) 1469–1497.

[6] H. Heavner, R.L Kumar, A.S. Wanniarachchci, Performance of an industrial plate heat exchanger: Effect of chevron angle, in: AIChE Symposium Ser. Heat Transfer, Am. Inst. Chem. Eng. Atlanta, GA, 1993.

[7] M.A. Mehrabian, R. Poulter, Hydrodynamics and thermal characteristics of corrugated channels: computational approach, Applied Mathematical Modeling 24 (2000) 343–364.

[8] M.Z. Hossain, A.K.M. Sadrul Islam, Numerical investigation of fluid flow and heat transfer characteristics in sine, triangular and arc-shaped channels, Thermal Science 11 (1) (2007) 17–26.

[9] Y. Asako, H. Nakamura, M. Faghri, Heat transfer and pressure drop characteristics in a corrugated duct with rounded corners, Int. J. Heat Mass Transfer 31 (6) (1988) 1237–1245.

[10] H.-M. Kim, K.-Y. Kim, Design optimization of rib-roughened channel to enhance turbulent heat transfer, Int. J. Heat Mass Transfer 47 (2004) 5159–5168.

[11] K.-Y. Kim, Y.-M. Lee, Design optimization of internal cooling passage with V-shaped ribs, Numerical Heat Transfer A 51 (2007) 1103–1118.

[12] J. Zhang, J. Kundu, R.M. Manglik, Effect of fin waviness and spacing on the lateral vortex structure and laminar heat transfer in wavy-plate-fin cores, Int. J. Heat Mass Transfer 47 (2004) 1719–1730.

[13] L. Wang, B. Sundén, Optimal design of plate heat exchangers with and without pressure drop specifications, Applied Thermal Engineering 23 (2003) 295–311.

[14] W.W. Focke, P.G. Knibbe, Flow visualization in parallel-plate ducts with corrugated walls, J. Fluid Mech. 165 (1986) 73–77.

[15] J.E. Hesselgraves, Compact Heat Exchangers: Selection, Design and Operation, 1st ed., Pergamon, New York, 2001.

[16] P. Vlasogiannis, G. Karagiannis, P. Argyropoulos, V. Bontozoglou, Air–water two-phase flow and heat transfer in a plate heat exchanger, Int. J. Multiphase Flow 28 (5) (2002) 757–772.

[17] A.G. Kanaris, A.A. Mouza, S.V. Paras, Flow and heat transfer in narrow channels with corrugated walls: a CFD code application, Chemical Engineering Research and Design 83 (A5) (2005) 460–468.

[18] A.G. Kanaris, A.A. Mouza, S.V. Paras, Flow and heat transfer prediction in a corrugated plate heat exchanger using a CFD code, Chemical Engineering and Technology 29 (8) (2006) 923–930.

[19] A. Bejan, A.D. Kraus, Heat Transfer Handbook, John Wiley and Sons, Inc., Canada, 2003.

[20] CFX® Release 10.0 Manual, ANSYS Inc. International, Canonsburg, 2005.

[21] Menter F., Esch T., Elements of industrial heat transfer predictions, in: 16th Brazilian Congress of Mechanical Engineering (COBEM), Uberlandia, Brazil, 2001.

[22] R.H. Myers, D.C. Montgomery, Response Surface Methodology: Process and Product Optimization Using Designed Experiments, 2nd ed., John Wiley & Sons Inc., Canada, 2002.

[23] G.E.P. Box, D.W. Behnken, Some new three level designs for the study of quantitative variables, Technometrics 2 (4) (1960) 455–475.

[24] Matlab 6.5 Manual, The Mathworks, Inc., 2002.

[25] H.-M. Kim, K.-Y. Kim, Shape optimization of three-dimensional channel roughened by angled ribs with RANS analysis of turbulent heat transfer, Int. J. Heat Mass Transfer 49 (2006) 4013–4022.

[26] M.A. Ansari, K.-Y. Kim, Shape optimization of a micromixer with staggered herringbone groove, Chem. Eng. Sci. 62 (2007) 6687–6695.

[27] M.E. Taslim, C.M. Wadsworth, An experimental investigation of the rib surface-averaged heat transfer coefficient in a rib-roughened square passage, Journal of Turbomachinery – Transactions of ASME 119 (2) (1997) 381–389.

[28] D.L. Gee, R.L. Webb, Forced convection heat transfer in helically rib-roughened tubes, Int. J. Heat Mass Transfer 23 (1980) 1127–1136.

[29] A. Bejan, Entropy Generation Through Heat and Fluid Flow, John Wiley and Sons, Inc., New York, 1982.